

Particle scale anisotropy controls bulk properties in sheared granular materials

Carmen L. Lee,¹ Ephraim Bililign,^{1,2} Emilien Azéma,^{3,4,5} and Karen E. Daniels¹

¹*Department of Physics, North Carolina State University, Raleigh, North Carolina, 27695, USA*

²*James Franck Institute and Department of Physics, University of Chicago, Chicago, IL, USA*

³*LMGC, Université de Montpellier, CNRS, Montpellier, France*

⁴*Department of Civil, Geological, and Mining Engineering, Polytechnique Montréal, Montréal, Canada.*

⁵*Institut Universitaire de France (IUF), Paris, France*

(Dated: May 2, 2024)

The bulk dynamics of dense granular materials arise through a combination of particle-scale and mesoscale effects. Theoretical and numerical studies have shown that collective effects are created by particle-scale anisotropic structures such as grain connectivity (fabric), force transmission, and frictional mobilization, all of which influence bulk properties like bulk friction and the stress tensor through the Stress-Force-Fabric (SFF) relationship. To date, establishing the relevance of these effects to laboratory systems has remained elusive due to the challenge of measuring both normal and frictional contact forces at the particle scale. In this study, we perform experiments on a sheared photoelastic granular system in an quasi-2D annular (Couette) cell. During these experiments, we measure particle locations, contacts, and normal and frictional forces vectors during loading. We reconstruct the angular distributions of the contact and force vectors, and extract the corresponding emergent anisotropies for each of these metrics. Finally, we show that the SFF relation quantitatively predicts the relationship between particle scale anisotropies, the stress tensor components, and the bulk friction coefficient, capturing even transient behaviors. As such, this method shows promise for application to other dense particulate systems where fabric anisotropy can provide a useful measure of bulk friction.

Foams, emulsions, colloidal suspensions, granular media, cellular tissues, and other amorphous materials all exhibit bulk phenomena that arise due to collective interactions, complicating the development of continuum models. Granular materials in particular have a poor separation of length scales, meaning that particle scale and mesoscale interactions heavily influence bulk properties [1–5]. Although bulk measures like stress, strain, or the bulk friction coefficient are well defined, the measured values vary because these properties are determined by the loading history. At best, continuum measures serve as ensemble information on the state of the granular material as a whole at that snapshot in time, rather than being a material property. In particular, it is well established that material strength arises from the buildup of various anisotropic structures at the particle scale, induced by grain connectivity (fabric), force transmission, and frictional mobilization [6–8].

Because fabric strongly influences bulk measures, even when the particles undergo identical loading history, jammed systems additionally exhibit an anisotropy in shear modulus [9, 10]. In rheological contexts, bulk friction coefficients have been shown to depend on the combination of fabric and force [11]. Theoretical micromechanical models have been developed to further understand granular material from rheology [12–14] to stability and jamming [15, 16] and many studies have quantified the anisotropic structures appearing while under load [17–21].

All of these challenges can be addressed with a framework first pioneered by Rothenburg and Bathurst [22], the Stress-Force-Fabric (SFF) relation connects the bulk

stress tensor to particle scale anisotropies in contact orientation, contact vector length, and force vectors; it has been verified extensively in DEM simulations of granular materials of varying complexity to understand the role of particle scale structure in bulk measurements [23–26]. Further work by Li and Yu [27] rigorously derived the SFF relation using a directional statistics approach and established the key assumptions. However, the SFF relation has seen little attention in laboratory systems because it requires measurements of individual particle contacts and vector forces. Recent developments in photoelastic techniques [28–30], combined with high-resolution photography now allows for force and contact resolution suitable to test the SFF relation using photoelastic granular assemblies.

In this study, we use photoelastic disks [28, 29] arranged in a single layer within an annular shear cell (Fig. 1(a)) to map emergent particle scale anisotropic structures to bulk friction and the stress tensor using the SFF relation and further apply it to capture dynamic behaviour. In doing so, we address the open question of the influence of particle scale anisotropy during granular dynamics and show the first laboratory demonstration of the SFF relation. The particles begin in an unstrained state with no observable forces and the inner boundary is rotated to shear the assembly. During these experiments, we record particle locations, contacts, and normal and frictional forces vectors for each particle and calculate the stress tensor and anisotropies from the packing information.

We performed experiments in a constant-area quasi-two-dimensional annular shear cell containing $N = 1810$

bidisperse (Vishay PhotoStress PSM-4) circular disks with an equal fraction of small particles with radii $R_s = 4.5$ mm and large particles with radii $R_l = 5.5$ mm ($R_l/R_s = 1.2$). The particles are dusted with baking powder to reduce basal friction between the particles and the supporting sheet, and the interparticle friction coefficient is estimated to be 0.3. The inner and outer boundaries of the annulus have particle-sized cavities to promote gripping between the boundaries and the packing while under shear. The inner boundary of the annulus is rotated at a constant rate of 1 rotation every 2.5 hours and the packing undergoes simple shear. Further details of the annulus can be found in previous works [31, 32]. Using the annular strain rate $\dot{\gamma} = \frac{1}{2} \left(\frac{\partial v}{\partial r} - \frac{v}{r} \right)$ as described by Tang *et al.* [33], and integrating over time with appropriate boundary conditions, we calculate the strain ϵ . The packing is illuminated with both red unpolarized light (particle-detection) and green circularly polarized light (darkfield polariscope). Images are taken at a frame rate of 5 seconds per frame with a Nikon D850 camera. We can extract particle position, contact and vector force data from the images of the particles as outlined in previous works [28, 29] by using the open source code, PhotoElastic Grain Solver [30] that we modified to detect particle-particle contacts with force magnitudes with a resolution of 5×10^{-5} N.

From the particle scale information, we calculate the

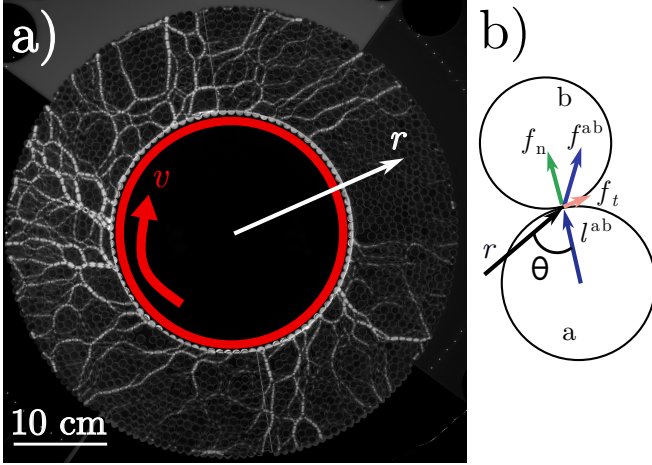


FIG. 1. (a) Top view of photoelastic particles viewed through a darkfield polariscope (white = higher stress) inside of an annular shear cell with inner boundary rotating at a constant velocity v and fixed outer boundary. Each particle provides a measurement of its own contact forces, which we measure relative to the contact position vector r . (b) Sketch of the interparticle coordinate system, with the branch vector l^{ab} pointing from the center of particle a to the contact point with particle b . The force exerted by particle a on b is given by f^{ab} ; this can be decomposed into normal f_n and tangential f_t . The angle θ defines the relative angle between l and r for the branch vector and position vector of the contact between particles a and b .

stress tensor in two dimensions using the micro-structural definition [34, 35]. We compute the two dimensional stress tensor via the summation of the outer product of the force \vec{f} and branch vectors \vec{l} [22, 27, 35],

$$\sigma_{ij} = \frac{1}{S} \sum_{a \neq b} l_i^{ab} f_j^{ab}, \quad (1)$$

where in our two dimensional system, S is the area of the annulus. Here we follow notation typical to the soil mechanics community, where the branch vector points from the center of the grain to the contact point, and the force vector points from the contact point in the direction of the contact force. Figure 1(b) shows a schematic of the vectors for two sample particles. From this formulation of the stress tensor, we are able to calculate the bulk friction coefficient,

$$\mu = \frac{\tau}{P} = \frac{\sqrt{(\sigma_{11} - \sigma_{22})^2 + 4\sigma_{12}\sigma_{21}}}{(\sigma_{11} + \sigma_{22})/2}, \quad (2)$$

where the numerator τ is the shear component of the stress tensor, and the denominator P is the pressure.

To consider the anisotropies in a granular material, the SFF relation relies on decomposing the stress tensor into angular distributions according to the branch vector normal \hat{n} . Assuming the thermodynamic limit, the stress tensor can be written as

$$\sigma_{ij} = \frac{zN}{S} \oint e^c(\hat{n}) \langle l_i f_j \rangle \hat{n}_j d\theta, \quad (3)$$

where z is the average contact number, N is the number of particles, θ is the angle corresponding to the normal vector relative to the position vector of the contact r , and $e^c(\hat{n})$ is the probability distribution of a contact appearing at a given normal vector. The SFF relation then takes the contact vector probability, average branch vector, and average force vector as a function of the contact angle, and expands it through a tensorial Fourier expansion. In the given system, which is composed of round particles, there is no directionality to the branch vector and therefore the branch vector is a scalar value determined by the average distance between two particles $l_0 = (N_s R_s + N_l R_l)/N$. Li and Yu [27] found that through the Fourier expansion the first rank Fourier coefficient is much larger than subsequent coefficients and the components of the stress tensor can be approximated as

$$E^c(\theta) = \frac{1}{2\pi} [1 + a \cos 2(\theta - \theta_a)], \quad (4a)$$

$$f_n(\theta) = f_0 [1 + a_n \cos 2(\theta - \theta_a)], \quad (4b)$$

$$f_t(\theta) = f_0 a_t \sin 2(\theta - \theta_a), \quad (4c)$$

where $E^c(\theta)$ is the probability density of contacts at a given angle, θ_a is the angle corresponding to the principle stress direction, f_0 is the average magnitude of the

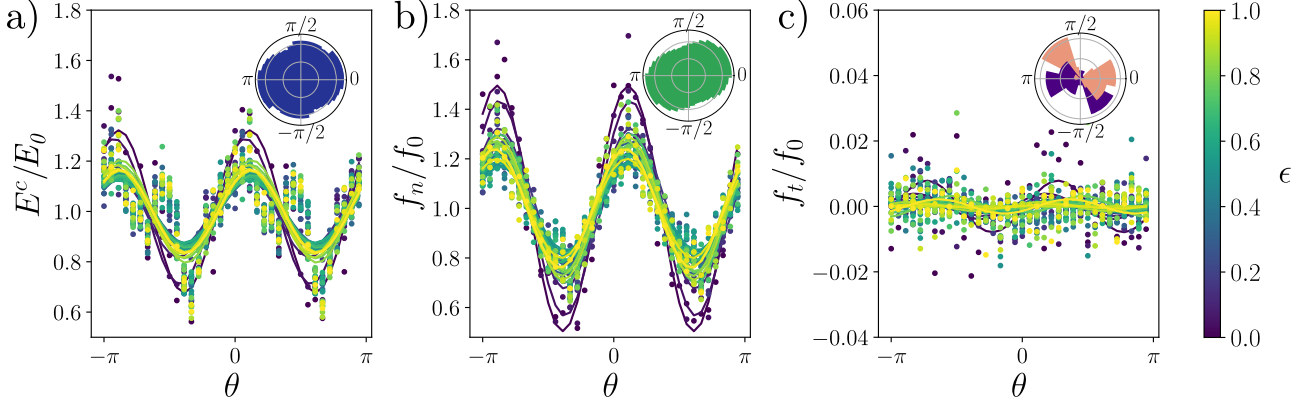


FIG. 2. Normalized angular distributions of the (a) contacts E^c , (b) normal forces f_n , and (c) tangential forces f_t at increasing levels of strain ϵ (dark purple to yellow). The contacts are normalized by the average number of contacts E_0 , and the forces are normalized by the average normal force f_0 at each given strain. Sample angular histograms of each anisotropic metric are shown in the respective insets, which have been averaged over the strain range shown in the main panel. $\theta = 0$ corresponds to the radial direction, and $\theta = \pi/2$ corresponds to the azimuthal direction. Fits to the respective Fourier expansions are indicated by the solid, sinusoidal line (Eqs. (4a)-(4c)). The normalized contacts and normalized normal forces show a decrease in anisotropy with increasing strain.

normal force, and θ is the relative angle between contact position vector and the branch vector (see Figure 1(b)). a, a_n, a_t are the leading order Fourier modes for the contact, normal force and tangential force distributions, respectively and can be considered as amplitudes of the anisotropy for the system.

Examples of the three distributions presented in Eqs 4a)-4c) are shown in Figure 2 with the contact distribution, normal forces and tangential forces in panels (a)-(c). Sample histograms averaged over strain $\epsilon = 0 - 1$ are shown in the inset as polar histograms. We plot the change in these anisotropic measures as a function of relative angle between the radial direction and branch vector, where $\theta = 0$ indicates alignment with the radial direction and $\theta = \pi/2$ indicates alignment with the azimuthal direction. We expect that the primary direction of the normal forces and contacts to align with the $\theta \sim \pi/4$ direction as the load is distributed through the shear band. This is true for the normal forces, indicating that the majority of the load is transmitted in the shear direction. The contact distribution follows a similar trend, however there is an additional secondary feature that appears as a bump aligned in the azimuthal direction $\theta = \pi/2$. Two possible reasons for the increased number of contacts near the azimuthal direction is either due to an artifact during contact detection, or an indication of a higher order Fourier mode, possibly present due to the constant area boundary condition. Regardless, this feature is small relative to the main signal, and we use only one Fourier mode to describe the data. The tangential distributions show only a weak signal above the noise, indicating that there is no strong preference for average tangential forces to be either clockwise (purple) or counterclockwise (pink) from the contact normal.

To quantify how the anisotropies evolve under ongoing strain, we consider the angular distributions at varying levels of strain. Figure 2 shows the normalized contact probability E_c , normalized normal force distribution f_n , and the normalized tangential forces f_t as a function of contact angle. The contacts are normalized by the mean number of contacts E_0 , and the forces normalized by the average normal force f_0 . The strain ranges from $\epsilon = 0 - 1$ indicated from purple (dark) to yellow (light) in increments of 0.04. As the assembly is strained, the amplitude of the sinusoidal shape decreases for the contacts (Fig. 2(a)) and normal forces (Fig. 2(b)).

Following the method of Li and Yu [27], we expand the stress tensor (Eq. 3) with the Fourier expansions of the three anisotropic metrics (Eqs. 4a-4c) to compare the particle scale anisotropies to bulk metrics. The SFF relation states that the stress tensor for a granular packing of isotropic particles in equilibrium can be written in terms of three main metrics: the angular contact angle distribution, and the average normal forces and average tangential forces:

$$\sigma_{ij} = \frac{zN}{2S} l_0 f_0 \left[(1 + a a_n) \delta_{ij} + \frac{1}{2} (a + a_n + a_t) \begin{pmatrix} \cos \theta_a & \sin \theta_a \\ \sin \theta_a & -\cos \theta_a \end{pmatrix} \right] \quad (5)$$

and this expansion of the stress tensor may be used to calculate the bulk friction coefficient μ . Inserting Eq. 5 into Eq. 2 results in a simple sum rule:

$$\mu = \frac{1}{2} (a + a_n + a_t), \quad (6)$$

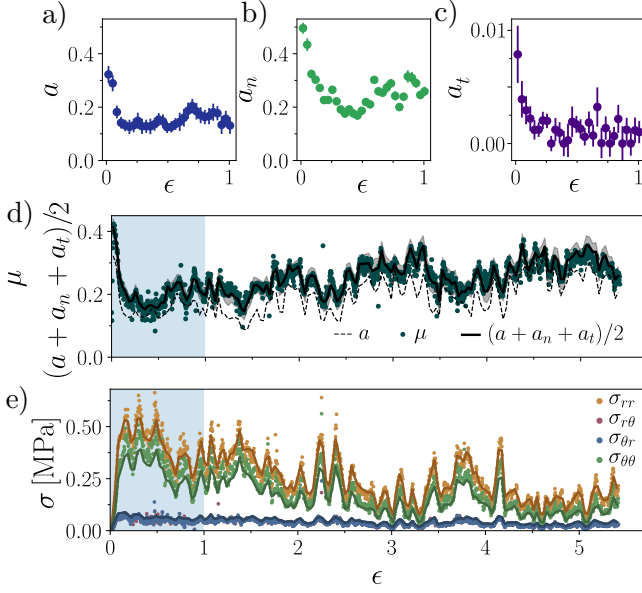


FIG. 3. Panels (a)-(c) display the leading term Fourier coefficients representing the angular distribution of contacts (a), average normal forces (a_n), and tangential forces (a_t), respectively, within a strained granular packing under shear. These coefficients quantify the degree of anisotropy observed in each metric within the packing. Panel (d) illustrates the bulk friction coefficient of the sheared granular packing as a function of shear, with the summed anisotropies overlaid in black and the standard error in the fit represented as grey filled bars spanning the best fit. The fabric anisotropy a is plotted with a black dashed line for comparison. The blue panel highlights the strain ϵ depicted in panels (a)-(c). Panel (e) presents the four components of the stress tensor, σ , as measured by Eq. 1, with principal and secondary stress axes oriented radially and azimuthally, respectively. The solid lines represent the stress tensor calculated from the anisotropies using Eq. 5.

which directly relates the bulk friction coefficient to the anisotropy measures, indicating that the resistance to deformation in a granular material simply depends on the amount of anisotropy that is present in the granular assembly.

To measure the level of anisotropy for the three metric values, we fit the angular distribution of contacts, normal forces and tangential forces (Fig. 2) to the predicted Fourier decomposition in Eqs. 4a-(c). We take the principle stress direction θ_a and the amplitudes a , a_n and a_t to be free fit parameters, where the anisotropy corresponds to the amplitudes. The anisotropies are plotted as a function of strain in Fig. 3(a)-(c); note that during the initial strain there is a strong decrease in value for all three metrics indicating a decrease in overall anisotropy. We also note that the relative magnitude of a and a_n are comparable which is consistent with simulated systems of disks [22, 36], and a_t is an order of magnitude smaller. This indicates that the tangential forces, and

consequently the inter-particle friction, has only a small effect in our system on the bulk friction, due to a_t being smaller than those reported in simulations [36, 37].

Comparing the two sides of Eq. 6 (Figure 3(d)), we see that there is excellent agreement between the two definitions of the stress tensor, the particle and bulk for a complete rotation of the inner boundary. For the annular shear cell used in these experiments, we expect μ to initially decrease as it undergoes strain softening before reaching a steady state [38]. Based on the SFF relation, this indicates that the fabric and forces are initially more strongly aligned before becoming more isotropic with increased strain. From the bulk definition, we expect that initially the assembly is resistant to shear before yielding after particle rearrangement. Furthermore, the anisotropies and bulk measurements also match each other well through large rearrangements and stick slip events, indicated by large spikes in μ . Notably, μ is not solely determined by the number of force chains (see supplemental video [39]), as there are strong fluctuations in the number of force chains for a given value of μ . We note that the SFF relation was developed for static loading conditions and although the dynamics in our systems are slow, the inertial number is small but non-zero ($I \sim 10^{-8}$) and there could be kinetic stress present in the system.

We gain further information from the simple shear packing by comparing the particle scale stress tensor with the bulk stress tensor. We plot the stress tensor components as measured by the force-moment tensor, as a function of strain, in Fig 3(e). The radial and azimuthal stress increase during straining, and then fluctuate as the particles undergo rearrangements during stick slip events. The off axis components of the stress tensor remain small. Overlaid on the calculated stress tensor components are the predictions for the stress tensor based on the anisotropic measures based on Eq. 5. These agree well with the measured values, however there tends to be a small discrepancy between the measured and predicted values. We attribute this discrepancy to rotations in the primary stress direction, especially during initial shear.

To explore the applicability of the SFF relation in the absence of photoelastic data, in Fig. 3(d) we show the effect of the fabric anisotropy alone by plotting only a as a function of strain (dashed black line). a follows the overall pattern of μ , including the initial transient and stick-slip events, but underestimates bulk friction by roughly 30%. Because a and a_n are typically of the same magnitude, while the tangential component is small, using the fabric anisotropy alone provides a good estimate of bulk friction.

In this study, we have shown experimental validation of the SFF relation using photoelastic particles in an annular shear cell. Success of the SFF relation indicates that the resistance to deformation of a granular material arises due to anisotropies in fabric and forces. Importantly, the

SFF relation remains valid even as transient stress builds up and releases through stick slip events, far beyond the static loading for which the framework was initially developed. We note that this framework does not address the role of mesoscale structure and therefore does not encompass prediction of rigidity [5]; however, the SFF relation is a promising pathway to address the open challenge of connecting fluid-like granular theories [12–14] to quasi-static granular behaviour. Finally, the framework may additionally provide a way to link fabric anisotropy to bulk friction in experimental systems for which vector contact forces cannot be measured, as illustrated by the success of the contact anisotropy a alone. We note that in the absence of force information, the geometric anisotropy provides a good estimate of bulk friction and could be easily applied to other deformable assemblies, including cellular tissues, foams, and dense colloid suspensions.

Acknowledgments: The authors thank Jonathan Barés and Tejas Murthy for fruitful discussions. C.L.L. acknowledges funding from the NSERC postdoctoral fellowship, and K.E.D and C.L.L from the National Science Foundation (DMR-2104986).

-
- [1] A. Tordesillas, S. D. C. Walsh, and B. S. Gardiner, *BIT Numerical Mathematics* **44**, 539 (2004).
 - [2] A. S. Keys, A. R. Abate, S. C. Glotzer, and D. J. Durian, *Nature Physics* **3**, 260 (2007).
 - [3] G. Shahin, E. B. Herbold, S. A. Hall, and R. C. Hurley, *Extreme Mechanics Letters* **51**, 101590 (2022).
 - [4] I. Goldhirsch, *Chaos: An Interdisciplinary Journal of Nonlinear Science* **9**, 659 (1999).
 - [5] K. Liu, J. E. Kollmer, K. E. Daniels, J. Schwarz, and S. Henkes, *Physical Review Letters* **126**, 088002 (2021).
 - [6] F. Radjai, J.-N. Roux, and A. Daouadji, *Journal of Engineering Mechanics* **143**, 04017002 (2017).
 - [7] T. Börzsönyi and R. Stannarius, *Soft Matter* **9**, 7401 (2013).
 - [8] X. Li and H.-S. Yu, *Acta Mechanica* **225**, 2345 (2014).
 - [9] S. Dagois-Bohy, B. P. Tighe, J. Simon, S. Henkes, and M. van Hecke, *Physical Review Letters* **109** (2012).
 - [10] B. Tighe, J. Snoeijer, T. J. Vlugt, and M. v. Hecke, *Soft Matter* **6**, 2908 (2010).
 - [11] F. da Cruz, S. Emam, M. Prochnow, J.-N. Roux, and F. Chevoir, *Physical Review E* **72**, 021309 (2005).
 - [12] P. Jop, Y. Forterre, and O. Pouliquen, *Nature* **441**, 727 (2006), publisher: Nature Publishing Group.
 - [13] K. Kamrin and G. Koval, *Physical Review Letters* **108**, 178301 (2012).
 - [14] D. Berzi, *Physical Review Fluids* **9**, 034304 (2024).
 - [15] M. E. Cates, J. P. Wittmer, J.-P. Bouchaud, and P. Claudin, *Physical Review Letters* **81**, 1841 (1998).
 - [16] C. S. Chang, Z.-Y. Yin, and P.-Y. Hicher, *Journal of Engineering Mechanics* **137**, 155 (2011).
 - [17] T. S. Majmudar and R. P. Behringer, *Nature* **435**, 1079 (2005).
 - [18] R. Wang, P. Fu, Z. Tong, J.-M. Zhang, and Y. F. Dafalias, *International Journal for Numerical and Analytical Methods in Geomechanics* **41**, 1758 (2017).
 - [19] J. Shi and P. Guo, *Acta Geotechnica* **13**, 1341 (2018).
 - [20] R. C. Hurley, S. A. Hall, J. E. Andrade, and J. Wright, *Physical Review Letters* **117**, 098005 (2016).
 - [21] D. Bi, J. Zhang, B. Chakraborty, and R. P. Behringer, *Nature* **480**, 355 (2011).
 - [22] L. Rothenburg and R. J. Bathurst, *Géotechnique* **39**, 601 (1989).
 - [23] E. Azéma, F. Radjaï, R. Peyroux, and G. Saussine, *Physical Review E* **76**, 011301 (2007).
 - [24] M. Cárdenas-Barrantes, D. Cantor, J. Barés, M. Renouf, and E. Azéma, *Physical Review E* **103**, 062902 (2021).
 - [25] W. Zhou and M. Xu, *Computers and Geotechnics* **165**, 105859 (2024).
 - [26] J. Liu, A. Wautier, F. Nicot, F. Darve, and W. Zhou, *International Journal of Solids and Structures* **252**, 111835 (2022).
 - [27] X. Li and H. S. Yu, *International Journal of Solids and Structures* **50**, 1285 (2013).
 - [28] A. Abed Zadeh, J. Bares, T. A. Brzinski, K. E. Daniels, J. Dijkman, N. Docquier, H. O. Everitt, J. E. Kollmer, O. Lantsoght, D. Wang, M. Workamp, Y. Zhao, and H. Zheng, *Granular Matter* **21**, 83 (2019).
 - [29] K. E. Daniels, J. E. Kollmer, and J. G. Puckett, *Review of Scientific Instruments* **88**, 051808 (2017).
 - [30] J. E. Kollmer, *Photo-Elastic Granular Solver (PEGS)* (2024).
 - [31] T. A. Brzinski and K. E. Daniels, *Physical Review Letters* **120**, 218003 (2018).
 - [32] F. Fazelpour and K. E. Daniels, *Soft Matter* **19**, 2168 (2023).
 - [33] Z. Tang, T. A. Brzinski, M. Shearer, and K. E. Daniels, *Soft Matter* **14**, 3040 (2018).
 - [34] N. P. Krut and L. Rothenburg, *Acta Mechanica* **225**, 2301 (2014).
 - [35] K. Bagi, *Journal of Applied Mechanics* **66**, 934 (1999).
 - [36] E. Azéma, S. Linero, N. Estrada, and A. Lizcano, *Physical Review E* **96**, 022902 (2017).
 - [37] T. Binaree, E. Azéma, N. Estrada, M. Renouf, and I. Preehawuttipong, *Physical Review E* **102**, 022901 (2020).
 - [38] J. Liu, A. Wautier, S. Bonelli, F. Nicot, and F. Darve, *International Journal of Solids and Structures* **193-194**, 222 (2020).
 - [39] <https://youtu.be/l7uvjusdv1g> (2024).